




A Novel Chimeric Oncolytic Virus Vector for Improved Safety and Efficacy as a Platform for the Treatment of Hepatocellular Carcinoma

Sarah Abdullahi,^a Melanie Jäkel,^a Sabine J. Behrend,^a Katja Steiger,^{b,c} Geoffrey Topping,^d Teresa Krabbe,^a Alessio Colombo,^e Volker Sandig,^f Tobias S. Schiergens,^g Wolfgang E. Thasler,^h Jens Werner,^g Stefan F. Lichtenthaler,^{e,i,j,k} Roland M. Schmid,^a Oliver Ebert,^a  Jennifer Altomonte^a

^aDepartment of Internal Medicine II, Klinikum rechts der Isar, Technische Universität München, Munich, Germany

^bDepartment of Pathology, Klinikum rechts der Isar, Technische Universität München, Munich, Germany

^cComparative Experimental Pathology, Klinikum rechts der Isar, Technische Universität München, Munich, Germany

^dDepartment of Nuclear Medicine, Klinikum rechts der Isar, Technische Universität München, Munich, Germany

^eGerman Center for Neurodegenerative Diseases (DZNE), Munich, Germany

^fProBioGen AG, Berlin, Germany

^gDepartment of General, Visceral, Vascular and Transplant Surgery, Hospital of the University of Munich, Munich, Germany

^hDepartment of General and Visceral Surgery, Red Cross Hospital, Munich, Germany

ⁱSchool of Medicine, Neuroproteomics, Klinikum rechts der Isar, Technical University of Munich, Munich, Germany

^jInstitute for Advanced Study, Technical University of Munich, Garching, Germany

^kMunich Cluster for Systems Neurology (SyNergy), Munich, Germany

ABSTRACT Oncolytic viruses represent an exciting new aspect of the evolving field of cancer immunotherapy. We have engineered a novel hybrid vector comprising vesicular stomatitis virus (VSV) and Newcastle disease virus (NDV), named recombinant VSV-NDV (rVSV-NDV), wherein the VSV backbone is conserved but its glycoprotein has been replaced by the hemagglutinin-neuraminidase (HN) and the modified, hyperfusogenic fusion (F) envelope proteins of recombinant NDV. In comparison to wild-type VSV, which kills cells through a classical cytopathic effect, the recombinant virus is able to induce tumor-specific syncytium formation, allowing efficient cell-to-cell spread of the virus and a rapid onset of immunogenic cell death. Furthermore, the glycoprotein exchange substantially abrogates the off-target effects in brain and liver tissue associated with wild-type VSV, resulting in a markedly enhanced safety profile, even in immune-deficient NOD.CB17-prkdc^{scid}/NCRcl (NOD-SCID) mice, which are highly susceptible to wild-type VSV. Although NDV causes severe pathogenicity in its natural avian hosts, the incorporation of the envelope proteins in the chimeric rVSV-NDV vector is avirulent in embryonated chicken eggs. Finally, systemic administration of rVSV-NDV in orthotopic hepatocellular carcinoma (HCC)-bearing immune-competent mice resulted in significant survival prolongation. This strategy, therefore, combines the beneficial properties of the rapidly replicating VSV platform with the highly efficient spread and immunogenic cell death of a fusogenic virus without risking the safety and environmental threats associated with either parental vector. Taking the data together, rVSV-NDV represents an attractive vector platform for clinical translation as a safe and effective oncolytic virus.

IMPORTANCE The therapeutic efficacy of oncolytic viral therapy often comes as a tradeoff with safety, such that potent vectors are often associated with toxicity,

Received 10 August 2018 **Accepted** 12 September 2018

Accepted manuscript posted online 19 September 2018

Citation Abdullahi S, Jäkel M, Behrend SJ, Steiger K, Topping G, Krabbe T, Colombo A, Sandig V, Schiergens TS, Thasler WE, Werner J, Lichtenthaler SF, Schmid RM, Ebert O, Altomonte J. 2018. A novel chimeric oncolytic virus vector for improved safety and efficacy as a platform for the treatment of hepatocellular carcinoma. *J Virol* 92:e01386-18. <https://doi.org/10.1128/JVI.01386-18>.

Editor Tom Gallagher, Loyola University Medical Center

Copyright © 2018 American Society for Microbiology. All Rights Reserved.

Address correspondence to Jennifer Altomonte, jennifer.altomonte@tum.de.

while safer viruses tend to have attenuated therapeutic effects. Despite promising preclinical data, the development of VSV as a clinical agent has been substantially hampered by the fact that severe neurotoxicity and hepatotoxicity have been observed in rodents and nonhuman primates in response to treatment with wild-type VSV. Although NDV has been shown to have an attractive safety profile in humans and to have promising oncolytic effects, its further development has been severely restricted due to the environmental risks that it poses. The hybrid rVSV-NDV vector, therefore, represents an extremely promising vector platform in that it has been rationally designed to be safe, with respect to both the recipient and the environment, while being simultaneously effective, both through its direct oncolytic actions and through induction of immunogenic cell death.

KEYWORDS chimeric virus, fusion protein, hepatocellular carcinoma, immunotherapy, oncolytic virus, syncytia

Hepatocellular carcinoma (HCC) is the second most common cause of cancer-related death worldwide (1), and the therapies that are currently available often provide only marginal survival benefits at the cost of undesirable side effects. In recent years, great progress has been made in the field of immune-based cancer therapy, offering the potential for safe, systemic, and long-lasting tumor responses. However, the complex and immune-suppressive microenvironment in the liver poses unique challenges, making HCC a particularly daunting therapeutic target. Oncolytic viruses (OVs) offer a novel approach to combat HCC, due to their inherent ability to cause direct tumor cell lysis while sparing the surrounding normal tissue (2–5), as well as their potential to stimulate potent immune responses directed against uninfected tumor cells and distant metastases (6, 7), resulting in an elegant multimodal therapy. OVs, therefore, represent an ideal platform to debulk the tumor, break immune tolerance, and launch powerful antitumor immune-mediated effects. The first approval of an oncolytic virus by the U.S. Food and Drug Administration in 2015 (8) has prompted a surge of interest in the OV field. With the growing enthusiasm and acceptance of OV therapies as promising cancer immunotherapeutics, the development of improved, next-generation OVs is now under intense investigation. With myriad OV platforms under development, an ongoing discussion in the field centers on the issue of which virus platforms are the most promising. Recently, the members of the subclass of OVs that encode a fusogenic protein have emerged as highly promising candidates due to their abilities to induce efficient viral spread and oncolysis, as well as immunogenic cell death (9).

The aim of facilitating clinical translation via virus-engineering strategies is to produce optimized oncolytic vectors that not only provide potent tumor cell-specific cytotoxic effects and stimulate antitumor immune responses but also demonstrate enhanced safety profiles. Unfortunately, in practice, it is difficult to achieve all of these goals with a single oncolytic construct, as safety and efficacy are often at odds, making it challenging to improve safety without compromising efficacy and vice versa. Among the most promising OV vector platforms under development are vesicular stomatitis virus (VSV) and Newcastle disease virus (NDV), both of which we have extensively characterized as therapeutics for HCC over the past decade (10–13). Despite promising preclinical data, the development of VSV as a clinical agent has been substantially hampered by the fact that severe neurotoxicity and hepatotoxicity have been observed in response to treatment with wild-type VSV (14–16). Furthermore, there has been a reported case of VSV-induced encephalitis in a child (17). In contrast, NDV has been shown to be a potent oncolytic agent with an attractive safety profile in humans in phase I and II clinical trials (18, 19). However, this virus poses an environmental and economic risk to the poultry industry, as it is a severe pathogen in its avian hosts. The mesogenic and velogenic strains of NDV were classified as select agents by the U.S. Department of Agriculture in 2008 (www.selectagents.gov), which has severely impeded the further clinical development of oncolytic NDV as a therapeutic agent.

A major benefit of NDV as an oncolytic virus is that, as a member of the paramyxovirus family, its viral envelope, comprising a hemagglutinin-neuraminidase (HN) and a

fusion (F) protein, mediates fusion of infected cells with their neighboring uninfected cells. This produces large multinucleated syncytia and thus provides a potent mechanism for viral spread and tumor cell killing via multimodal responses. As part of the virus life cycle, the translated viral glycoproteins become embedded in the host cell membrane, allowing newly produced virions to become incorporated in their envelopes through the process of budding from the cell. Viral fusion proteins that are exposed to the cell surface of infected cells also trigger fusion with plasma membranes of neighboring cells, leading to a chain reaction in which a single virion can potentially infect and kill dozens of surrounding cells by pulling them into the growing syncytium. In addition to fusion being a potent mechanism of intracellular virus spread and tumor cell killing, this mechanism of cell death by syncytium formation has now been fittingly characterized as immunogenic cell death (ICD) (20). Infected cells expose several proinflammatory danger signals, including calreticulin (CRT) on the plasma membrane (ecto-CRT), as well as the release of ATP, high-motility group box 1 (HMGB1), and heat shock proteins 70 and 90 (Hsp70 and Hsp90) (21). These danger signals activate dendritic cells (DCs), which in turn cross-present tumor-associated antigens (TAAs) released by dying cells to cytotoxic CD8⁺ T cells, thereby stimulating adaptive antitumor immune responses (22). We have previously demonstrated that the incorporation of a modified, highly fusogenic fusion protein [F3aa(L289A)] from NDV into the oncolytic VSV backbone resulted in enhanced intratumoral viral spread and significant survival prolongation in orthotopic HCC-bearing rats (10, 23), as well as in head and neck squamous cell carcinoma (24). However, because the attachment of this vector is directed solely by the endogenous VSV glycoprotein, the tropism of the vector was not altered compared to wild-type VSV. The transgene expression of NDV-F had the singular function of causing the virus to induce fusion but had no effect on reducing off-target effects, and the maximum tolerated dose was unaltered compared to the parental rVSV vector (23).

Considering the positive and negative features of both VSV and NDV as oncolytic virus platforms, we envisioned an optimized hybrid vector construct which would include the beneficial elements of each virus but not the virus's respective safety issues. We engineered a chimeric virus based on the rapidly replicating VSV backbone, in which the tropism was altered by replacing the endogenous glycoprotein with NDV's envelope proteins. The key difference between this chimeric virus and the previously reported modified NDV-F(L289A) protein vector (referred to here as "rVSV-F") is that rVSV-NDV does not encode the endogenous VSV glycoprotein G protein; therefore, the neurotropism and hepatic tropism associated with targeting via VSV-G were ameliorated. Instead, rVSV-NDV expresses the NDV HN protein, which mediates cellular attachment of the virus in the absence of VSV-G and thereby alters the tropism of the virus.

Here we demonstrate for the first time that the chimeric rVSV-NDV vector causes rapid and efficient syncytium formation in human HCC cell lines, with significantly reduced cytotoxicity in healthy hepatocytes and neurons and no pathogenicity in embryonated chicken eggs. This hybrid vector exhibits a substantial reduction in toxicity in immunocompromised NOD.CB17-prkdc^{scid}/NCrCrI (NOD-SCID) mice, with an elevation in the MTD by at least 1,000-fold compared to rVSV. The therapeutic effect is potentially further enhanced through induction of immunogenic cell death, and we demonstrate that the survival of orthotopic HCC-bearing mice could be significantly prolonged by rVSV-NDV treatment, even when administered via systemic injection, which is a notoriously inefficient administration route for oncolytic viruses. These findings support the idea of the further development of rVSV-NDV for clinical translation as a novel vector platform for cancer immunotherapy for HCC.

RESULTS

Rescue and characterization of rVSV-NDV. To create the rVSV-NDV hybrid construct, VSV glycoprotein G (VSV-G) was deleted from a plasmid carrying the full-length VSV genome. To achieve protein levels for the NDV envelope proteins similar to those achieved by the endogenous G, cDNAs encoding the modified NDV fusion protein

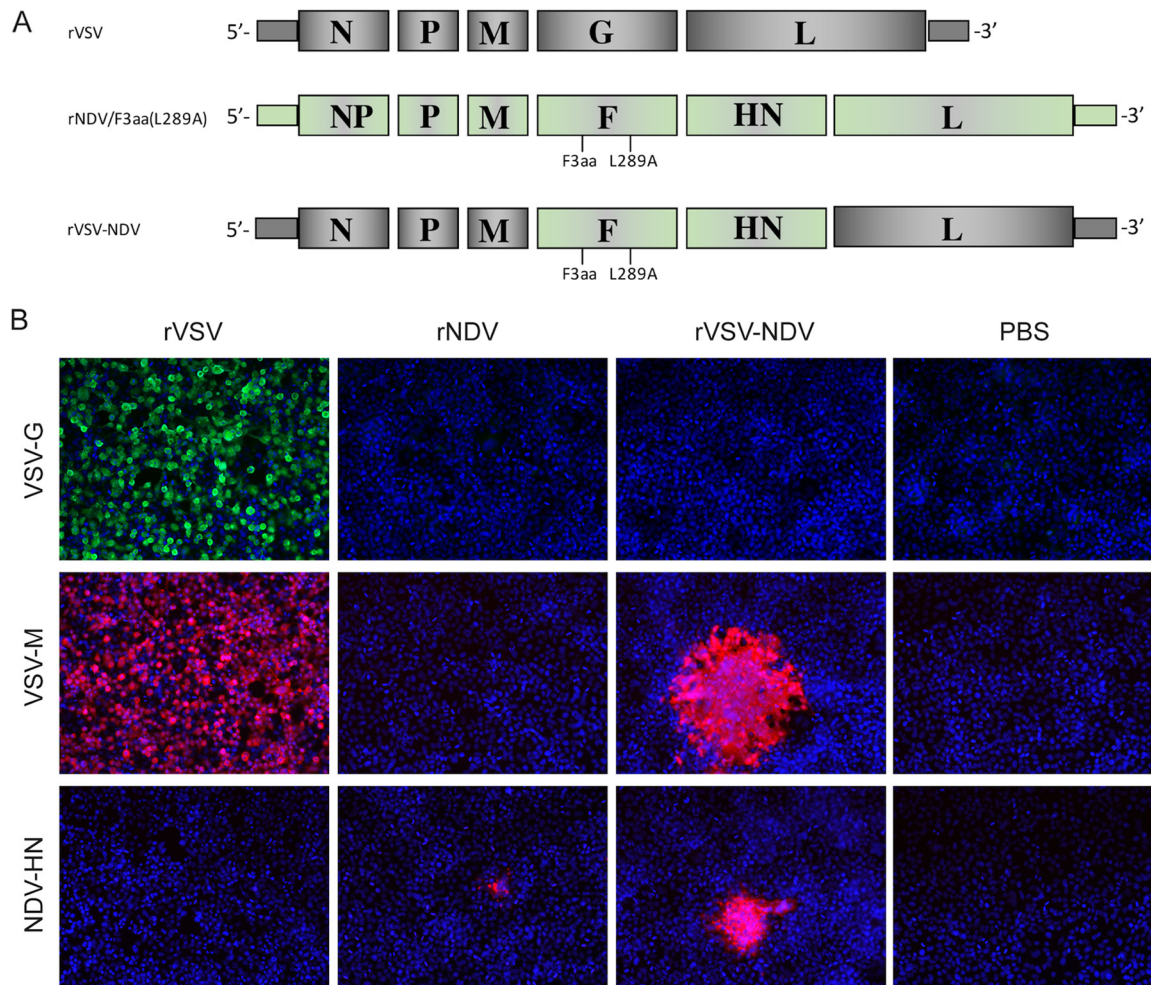


FIG 1 Construction and *in vitro* characterization of the hybrid rVSV-NDV virus. (A) The endogenous glycoprotein of VSV was deleted from a plasmid carrying the full-length VSV genome. The NDV glycoproteins, comprising a modified fusion protein [NDV/F3aa(L289A)] and the hemagglutinin-neuraminidase protein (NDV/HN), were inserted as discrete transcription units between the VSV matrix (M) and large polymerase (L) genes. The genomes of rVSV, rNDV/F3aa(L289A), and rVSV-NDV are shown. The chimeric VSV-NDV vector was rescued using an established reverse-genetics system. (B) Expression of viral genes was confirmed by indirect immunofluorescence analysis. Huh7 cells were mock infected or infected with rVSV or rNDV or rVSV-NDV at an MOI of 0.001 for 24 h. Immunofluorescence analysis was performed using primary antibodies against VSV-G, VSV-M, or NDV-HN and the appropriate fluorescence-labeled secondary antibodies. Cells were counterstained with DAPI (4',6-diamidino-2-phenylindole) for localization of nuclei. Representative fields of view are shown at $\times 400$ magnification.

[F3aa(L289A)] and the hemagglutinin neuraminidase (HN) protein were cloned into the site formerly occupied by VSV-G (Fig. 1A). The gene order of F and HN as they naturally occur in the NDV genome was conserved. After applying the established reverse genetics system, we were able to observe syncytia in BHK-21 monolayers. The rescued virus was characterized *in vitro* by indirect immunofluorescence, whereby rVSV-NDV-infected Huh7 cells were compared to uninfected cells and those infected with rVSV and recombinant NDV harboring the F3aa(L289A) mutation and expressing the GFP reporter gene [rNDV/F3aa(L289A)-GFP] (referred to here as "rNDV"). As expected, cells infected with the newly rescued rVSV-NDV vector did not express the VSV-G, although expression of the VSV matrix protein (M) was maintained, and cells additionally expressed the NDV-HN protein in their cytoplasm and cell membranes (Fig. 1B). In contrast, cells infected with the control rVSV alone expressed the VSV-G and VSV-M proteins, while infection with rNDV alone led to positive staining for the NDV-HN protein. Unfortunately, we do not know of a commercially available antibody that is able to detect the NDV-F protein by immunofluorescence. However, further analysis of the immunofluorescent images reveals that, while VSV infection produces a classical

cytopathic effect (CPE) throughout the monolayer, infection of cells with rVSV-NDV seems to spread intracellularly in a pattern consistent with fusion-mediated syncytium formation. Furthermore, the presence of the F gene was confirmed by reverse transcription-PCR (RT-PCR) analysis of RNA isolated from infected cells (data not shown).

rVSV-NDV can replicate in human HCC cells and cause efficient cytotoxicity. In order to assess the ability of the hybrid rVSV-NDV vector to replicate in HCC cells, we utilized the Huh7 and HepG2 human HCC cell lines as representative tumor cells and compared rVSV-NDV with rVSV and rNDV in terms of their relative abilities to replicate and kill the cells. Interestingly, although rVSV-NDV replication was highly attenuated compared to the levels seen with the parental VSV and NDV vectors, with titers up to 4-logs lower than the VSV levels, this minimal amount of viral replication of rVSV-NDV was sufficient to result in complete cell killing *in vitro* within 72 h after an infection at a multiplicity of infection (MOI) of 0.01 (Fig. 2A). Although lactate dehydrogenase (LDH) assays seemed to demonstrate a slightly reduced level of cytotoxicity at early time points after infection with rVSV-NDV compared to the parental viruses, we believe this to be an artifact of the assay, rather than a reflection of a delayed response to the virus. This interpretation is supported by microscopic analysis of infected Huh7 cells performed at different time points postinfection, in which we observed clear syncytium formation as early as 18 h postinfection (as indicated by arrows in Fig. 2B) and complete destruction of the monolayers by 48 h after infection at an MOI of 0.01. Compared to cells infected with the parental viruses under the same circumstances, the observed cytopathic effects occurred more rapidly than in rNDV-infected cells and at a rate similar to that achieved in rVSV-infected cells. (Fig. 2B). Comparable results were observed in infected HepG2 cells (data not shown). These results indicate that rapid induction of cell-cell fusion, leading to extensive syncytial spread, is a highly efficient mechanism of OV-mediated killing, which potentially bypasses the need for high levels of virus replication.

VSV vectors induce various patterns of cytopathic effects depending on the combination of VSV and NDV glycoproteins expressed. In order to observe the effect of glycoprotein exchange or additional glycoprotein expression in the context of VSV replication and spread, we infected Huh7 cells with the following VSV constructs at an MOI of 0.01: rVSV (encoding the wild-type VSV genome, including the endogenous VSV-G), rVSV-F (in which the modified NDV F protein is expressed as a transgene in addition to the endogenous VSV-G [23]), and rVSV-NDV (where the VSV-G has been exchanged with NDV envelope proteins F and HN). Microscopic analysis at 24 h postinfection revealed very different morphologies of cell death, depending on which virus vector was used (Fig. 3A). While rVSV resulted in classical cytopathic effect (CPE) by cell rounding, rVSV-F caused two distinct patterns of cell death: cell rounding and syncytium formation. In contrast, infection with rVSV-NDV resulted in cell death exclusively via syncytium formation. This demonstrates that the deletion of VSV-G completely abrogates the classic CPE mediated by VSV and that the chimeric VSV-NDV vector is, therefore, able to spread only by cell-cell fusion. In line with the microscopic analysis, virus growth curves revealed that rVSV-F replicated to slightly higher titers than rVSV, while rVSV-NDV replication was highly attenuated compared to that seen with both of the other viruses (Fig. 3B). Cytotoxicity data, as determined by LDH assay, similarly revealed that rVSV-F caused slightly faster and more potent tumor cell killing than rVSV, although these results were not statistically significant (Fig. 3C).

Retargeting VSV with NDV envelope proteins does not alter the sensitivity of the vector to the antiviral actions of IFN and results in substantial attenuation in healthy hepatocytes and neurons. In order to rule out the possibility that the glycoprotein exchange inadvertently resulted in a loss of sensitivity of the vector to the antiviral actions of type I interferon (IFN), an IFN protection assay was performed. The exquisite sensitivity of VSV to type I IFN is a key mechanism of tumor specificity, as tumor cells are often defective in their IFN signaling pathways, while healthy cells can efficiently clear the virus via IFN-responsive genes. To assess the sensitivity of rVSV-NDV to type I IFN, an IFN-sensitive cell line (A549) was pretreated

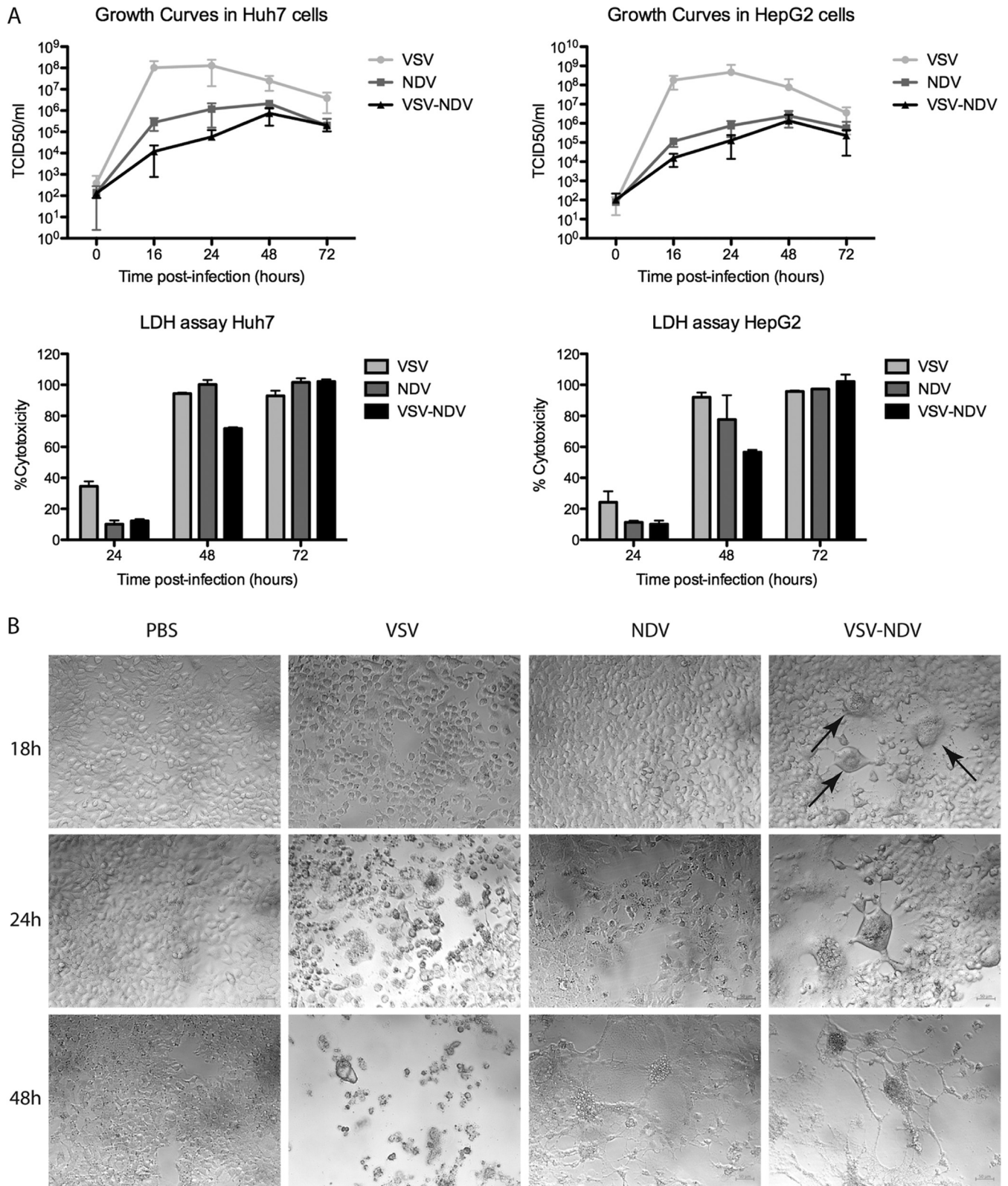


FIG 2 rVSV-NDV can replicate in HCC cell lines and cause complete cytotoxicity. (A) Human HCC cell lines (Huh7 [left] and HepG2 [right]) were infected with rVSV or rNDV or rVSV-NDV at an MOI of 0.01. Cell monolayers were lysed at various time points postinfection for intracellular titer measurement by TCID₅₀ analysis. At the same time, aliquots of the supernatant were collected to quantify cytotoxicity using an LDH assay. Experiments were performed in triplicate, and data are presented as means ± standard deviations. (B) Additional Huh7 cells were mock infected or infected with rVSV or rNDV or rVSV-NDV at an MOI of 0.01, and photomicrographs of cell monolayers were captured at various time points postinfection at ×200 magnification (bottom panels). Arrows indicate early syncytial formation. Representative fields of view are shown.

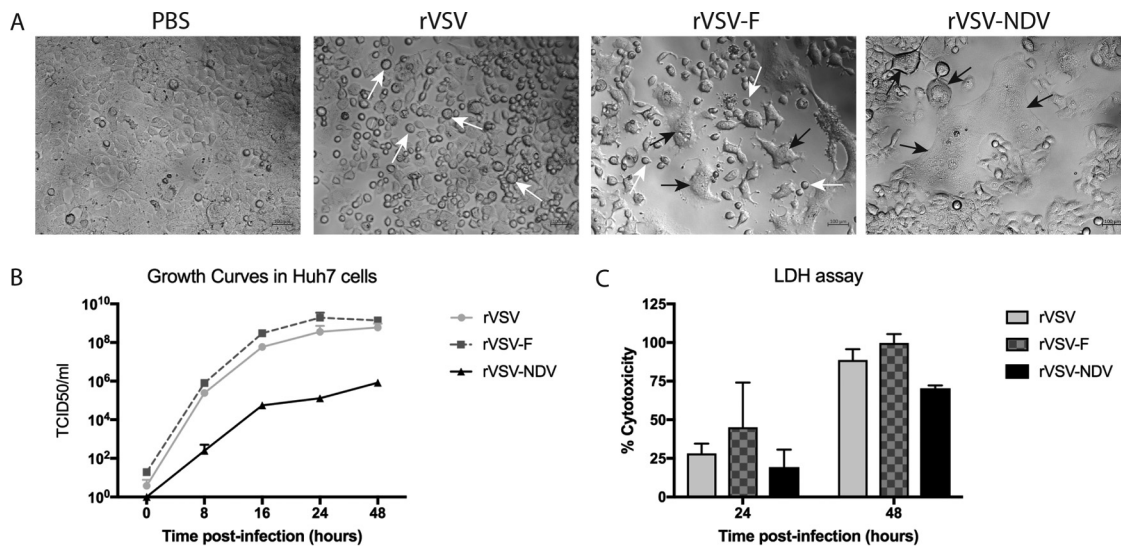


FIG 3 Adjusting the combination of glycoproteins expressed by VSV results in altered patterns of virus spread and tumor cytotoxicity. (A) Huh7 cells were mock infected or infected with rVSV or rVSV-F or rVSV-NDV at an MOI of 0.01. Representative photomicrographs were captured at $\times 400$ magnification at 24 h postinfection to compare the patterns of virus-mediated cytopathic effects. Scale bars = 100 μ m. (B) Aliquots of supernatants from Huh7 cells were collected at the indicated time points after infection with rVSV or rVSV-F or rVSV-NDV at an MOI of 0.01 and subjected to TCID₅₀ analysis of virus titers. (C) Additional aliquots of supernatant were used for quantification of cytotoxicity by LDH assay. Mean values and standard errors of the means (SEM) representative of results of 2 individual experiments performed with triplicate samples are shown.

with increasing doses of universal type I IFN prior to infection with rVSV-NDV, rVSV, or rNDV at an MOI of 0.01. Although this assay revealed a relative insensitivity of rNDV to type I IFN, which is contradictory to our previous findings (11), the rVSV-NDV vector was clearly attenuated by the addition of IFN, irrespective of the applied IFN dose, and titers were reduced to levels similar to those observed for rVSV (Fig. 4A).

To further assess the tumor specificity of rVSV-NDV, we next plotted growth curves and performed cytotoxicity assays in normal primary human hepatocytes (PHH) and healthy mouse neurons. Very little replication of the pseudotyped vector could be observed in either cell type over time, and the titers were approximately 5 logs lower than the control VSV vector titers at 48 h postinfection and 3 logs lower than the rNDV titers corresponding to the same time point in primary hepatocytes (Fig. 4B and C). Although nearly all hepatocytes were dead by 72 h postinfection with rVSV, almost no cytotoxicity could be observed by LDH assay in cells infected with rVSV-NDV (P value for rVSV-NDV versus rVSV at 72 h, <0.05) (Fig. 4B), representing a level which was significantly reduced compared even to that seen with rNDV, which is not known to be hepatotoxic ($P = <0.05$). While rVSV caused rapid cytotoxicity in primary neurons, both rNDV treatment and rVSV-NDV treatment led to significantly higher cell viability at all time points investigated ($P < 0.05$) (Fig. 4C) and produced no signs of syncytia (data not shown). Taking the data together, rVSV-NDV showed little evidence of replication or cytopathic effects in primary healthy cells *in vitro*, indicating that off-target replication was greatly diminished compared to rVSV replication.

The chimeric VSV-NDV virus is nonvirulent in embryonated chicken eggs. In order to characterize the pathogenicity of rVSV-NDV in birds, we performed a standard mean death time (MDT) assay in embryonated chicken eggs. Eggs were inoculated with increasing doses of rVSV-NDV or of recombinant NDV control vectors expressing the green fluorescent protein (GFP) reporter (rNDV-GFP) in order to determine the minimum lethal dose (MLD) and MDT of each. These values were used to determine the pathogenicity classification of each virus. Consistent with our previous findings, rNDV-GFP caused an MDT of approximately 80 h, corresponding to a mesogenic (moderately pathogenic) classification. In contrast, rVSV-NDV did not result in complete lethality of

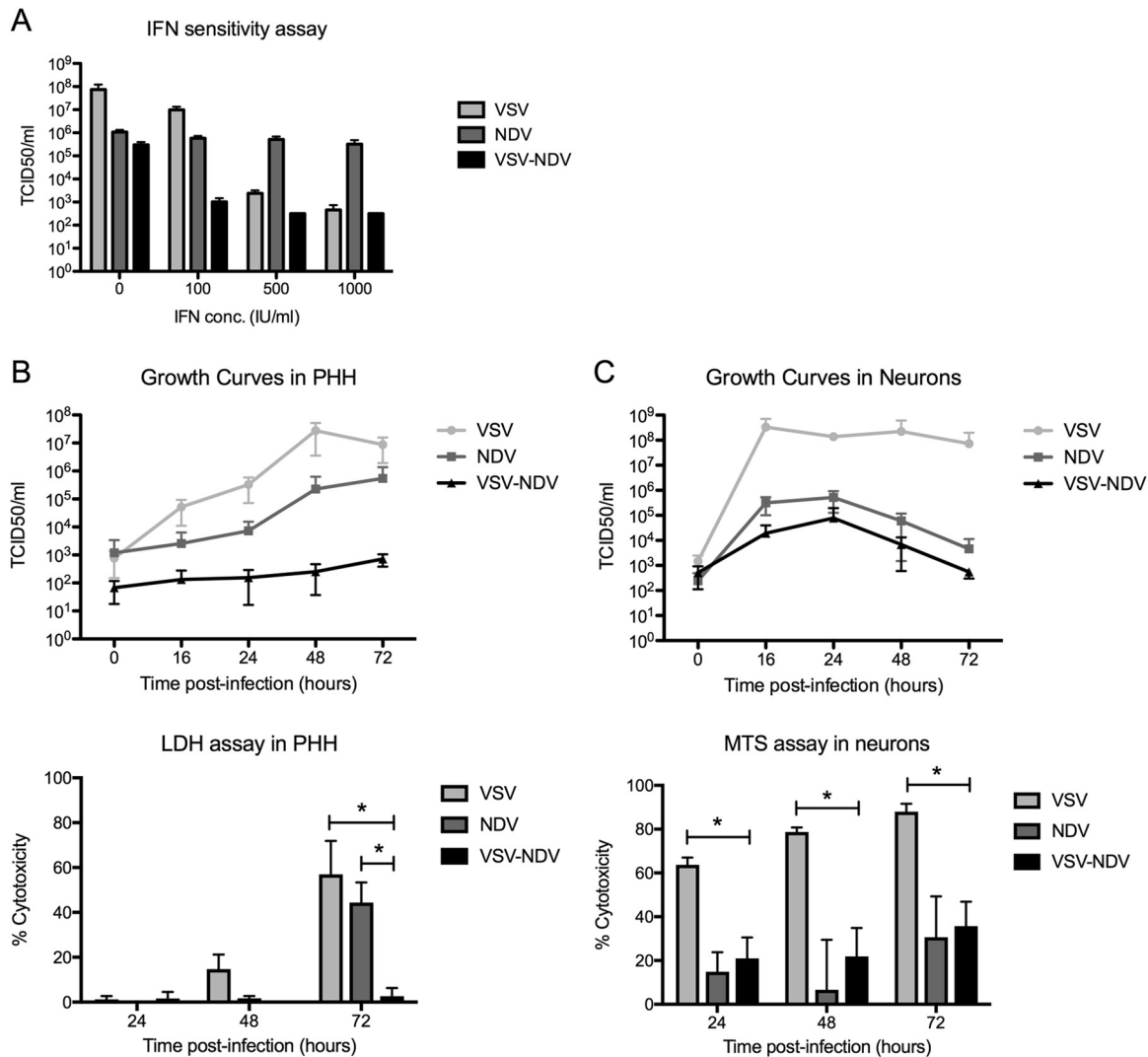


FIG 4 rVSV-NDV is sensitive to antiviral type I interferon, and its replication and cytotoxicity are attenuated in healthy hepatocytes and neurons. (A) IFN-sensitive A549 cells were infected with rVSV or rNDV or rVSV-NDV at an MOI of 0.01. Cells were lysed at 48 h postinfection, and intracellular viral titers were measured by TCID₅₀ analysis. Experiments were performed in triplicate, and mean values \pm standard errors of the means of the results are shown. (B and C) Primary human hepatocytes (B) or primary embryonic mouse neurons (C) were infected at an MOI of 0.01 with rVSV, rNDV, or rVSV-NDV. Cell lysates were subjected to TCID₅₀ analysis of intracellular virus titers at various time points. Additionally, aliquots of supernatant were collected at various time points to quantify cytotoxicity using either an LDH assay (for hepatocytes) or an MTS assay (for neurons). Experiments were performed in triplicate, and means \pm standard errors of the means of the results are shown. *, $P < 0.05$.

embryos, even at the highest inoculated dose tested (10^4 50% tissue culture infective doses [TCID₅₀]), making it impossible to determine an MDT within the 7-day duration of the assay. These findings indicate that the chimeric VSV-NDV vector can be classified as lentogenic, or nonvirulent, in avian species. The results of this assay are summarized in Table 1.

Virus-mediated syncytium formation in HCC cells leads to immunogenic cell death. As syncytium formation is known to cause immunogenic cell death (ICD), we aimed to demonstrate that the replacement of VSV's glycoprotein G with the fusogenic envelope proteins of NDV would lead to an induction of ICD that could potentially contribute to immune-mediated therapeutic effects of the virus *in vivo*. To this end, Huh7 cells were mock infected or infected with rVSV, rNDV, or rVSV-NDV for 24 h and analyzed for the expression of various ICD markers, namely, the release of ATP, high-mobility group box 1 (HMGB1), and heat shock proteins 70 and 90, as well as for the surface exposure of calreticulin (ecto-CRT). In an immunofluorescent assay, we

TABLE 1 Mean death time assay

Inoculated dose (TCID ₅₀)	VSV-NDV death time (h) ^a					NDV-GFP death time (h) ^b				
	1	2	3	4	5	1	2	3	4	5
10										
100			168			88	88	72	88	72
1,000	168	168				72	88	65	65	88
10,000	168					65		65	65	65

^aMinimum lethal dose (MLD), not applicable (NA); mean death time (MDT), NA; classification, lentogenic/nonvirulent.

^bMLD, 100 TCID₅₀; MDT, 81.6 h; classification, mesogenic.

observed substantially enhanced expression of ecto-CRT in rNDV- and rVSV-NDV-infected Huh7 cells compared to mock- or rVSV-infected cells. Ecto-CRT colocalized with cell membranes stained with CellMask Deep Red (Fig. 5A). Furthermore, significantly higher concentrations of ATP were measured in the supernatants of rVSV-NDV-infected cells than in those of cells in any of the other treatment groups (Fig. 5B). While relatively low levels of HMGB1, Hsp70, and Hsp90 were released into the supernatant of rVSV-infected cells, infection with both rNDV and rVSV-NDV resulted in high levels of all three secreted markers for immunogenic cell death, as detected by Western blotting (Fig. 5C). Taken together, these results indicate that, in addition to the potent direct cytotoxicity caused by infection with the chimeric rVSV-NDV vector, *in vivo* treatment with this virus could provide the additional benefit of enhanced immune responses directed against the tumor, mediated by ICD.

rVSV-NDV demonstrates enhanced safety compared to rVSV in immunodeficient mice. In order to assess the safety of the pseudotyped rVSV-NDV vector *in vivo*,

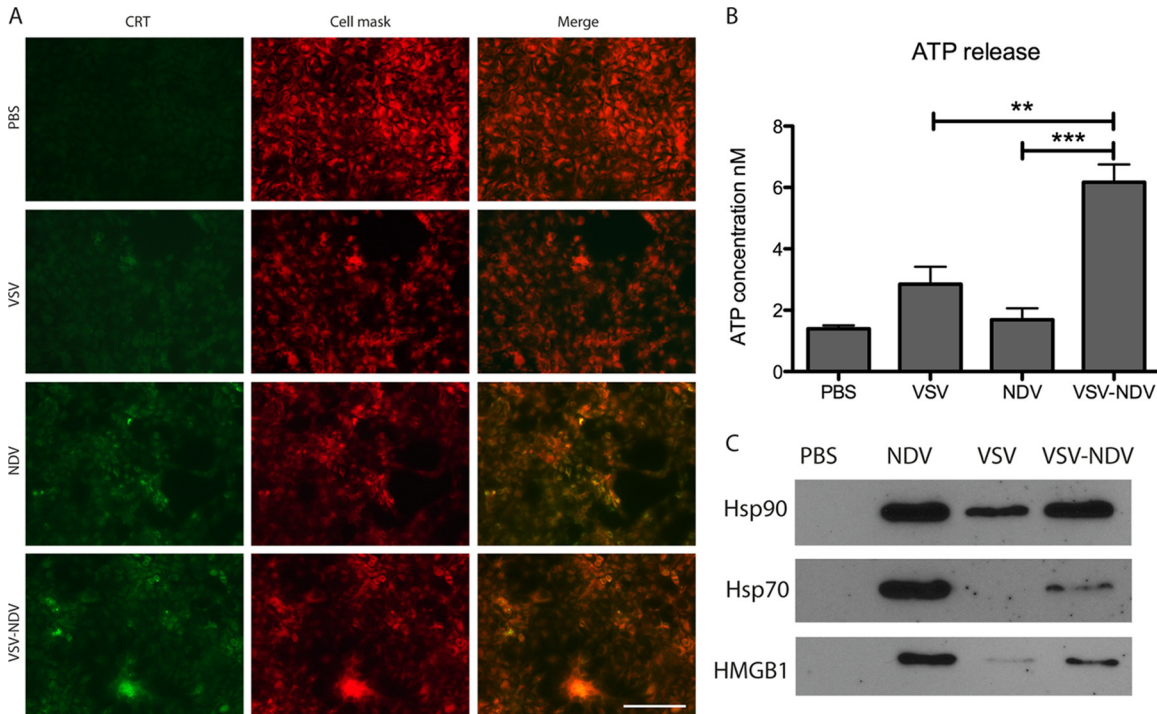


FIG 5 The chimeric rVSV-NDV vector causes immunogenic cell death. Huh7 cells were mock infected (PBS) or infected with rVSV, rNDV, or rVSV-NDV at an MOI of 0.01 for 24 h. (A) Monolayers were analyzed for ecto-calreticulin (CRT) (green) by indirect immunofluorescence analysis. Cell membranes were localized using CellMask staining (red). Representative sections with single stainings and merged images are shown at $\times 400$ magnification. Scale bar = 100 μ m. (B) Aliquots of conditioned medium were collected and subjected to ATP measurement using a standard kit. The experiment was performed in triplicate, and means \pm standard errors of the means of the results are shown (**, *P* value for rVSV-NDV versus VSV, <0.005 ; ***, *P* value for rVSV-NDV versus NDV, <0.0005). (C) The conditioned media collected 48 h postinfection at an MOI of 0.01 were concentrated, and 10 μ g of protein samples was subjected to Western blot analysis for detection of released HMGB1, Hsp70, and Hsp90.

immune-deficient male NOD-SCID mice were randomized for treatment by tail vein injection with either rVSV-NDV or the control rVSV-GFP virus at increasing doses in log increments. Immune-deficient mice were chosen for this study, since they are known to be extremely susceptible to VSV, and any improvement in safety could therefore be easily identified in this model. A traditional 3-plus-3 Fibonacci dosing scheme was applied, in which 3 mice are initially assigned to each dose level, and in the case of dose-limiting toxicity (DLT), 3 additional mice can be added to that dose level. If no additional DLTs occur at that dose, the dose is considered safe. Mice were monitored daily for body weight and overall physical appearance, and they were euthanized at humane endpoints. All mice treated with rVSV at doses of 10^5 TCID₅₀ and higher experienced outward signs of toxicity, including excessive weight loss, altered posture, and neurological issues such as circling and limb paralysis (summarized in Fig. 6A). Histological evaluation of tissue extracted upon necropsy from these mice revealed heavy intrasinusoidal edema, moderate acute hepatitis with single-cell and small-group necrosis, and apoptosis of hepatic tissue, as well as acute necrosis in the brain stem, with degenerating glial cells exhibiting pyknosis and karyorrhexis (Fig. 6B). TCID₅₀ analysis of tissue lysates revealed quantifiable levels of infectious VSV in the liver and brain (Fig. 6B). Mice treated with 10^4 TCID₅₀ of rVSV did not show any outward alterations in appearance or body weight and remained healthy throughout the study. Therefore, the maximum tolerated dose (MTD) of rVSV in NOD-SCID mice was determined to be 10^4 TCID₅₀. In contrast, doses of up to 10^6 TCID₅₀ of rVSV-NDV were well tolerated without the onset of any alterations in health status or body weight (Fig. 6A). Injection of 10^7 TCID₅₀ led to toxicities in one mouse (body weight loss and overall poor appearance) in the first group of 3 mice treated at this dose. Investigations with 3 additional mice treated at the same dose of rVSV-NDV revealed no further toxic events. Histological examination of liver and brain revealed no abnormal pathological signs, and no infectious virus could be recovered from the blood, liver, or brain upon euthanasia, indicating that no viremia had occurred. Plasma measurements of liver function (glutamate-pyruvate transaminase [GPT]) and kidney function (blood urea nitrogen [BUN] and creatinine) were within normal range, and histological examination of liver and brain revealed no abnormal findings. We therefore determined 10^7 TCID₅₀ to be a safe dose for rVSV-NDV in this model. Based on these data, we can summarize that the MTD of rVSV-NDV is elevated at least 1,000-fold in immune-deficient NOD-SCID mice compared to rVSV (10^7 versus 10^4 TCID₅₀).

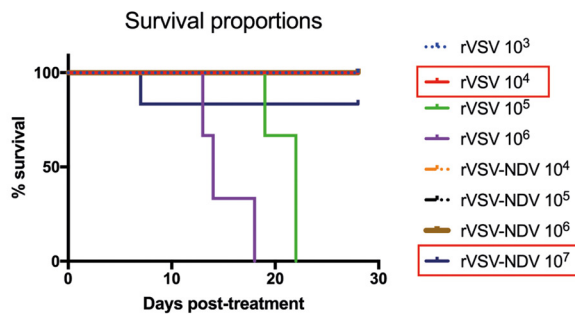
Tail vein injection of rVSV-NDV results in a doubling of the mean survival time in orthotopic HCC-bearing mice. To assess a potential therapeutic benefit of the chimeric VSV-NDV construct as an oncolytic agent, orthotopic, multifocal HCC lesions were induced in immunocompetent AST mice (Fig. 7). After confirmation of intrahepatic tumors, tail vein injections of rVSV or rVSV-NDV, at a dose of 10^7 TCID₅₀, or of phosphate-buffered saline (PBS) were administered twice with a 1-week interval between injections. Mice were monitored regularly, and survival times posttreatment were plotted. Not surprisingly, rVSV-GFP was not effective in prolonging survival compared to PBS treatment ($P > 0.5$), most likely due to the relatively low tumor transduction efficiency of viruses injected via systemic tail vein injection of virus, a phenomenon which is well accepted in the field. In contrast, treatment with rVSV-NDV resulted in statistically significant ($P < 0.005$) survival prolongation compared to PBS treatment (Fig. 7C). Strikingly, the median survival time was nearly doubled in the rVSV-NDV treatment group compared to the PBS treatment group (35 days versus 18 days). Whether the survival prolongation afforded by systemically administered rVSV-NDV was primarily mediated by direct oncolytic effects or via immune-stimulatory responses could not be determined in this experiment and will be investigated closely in follow-up mechanistic studies.

DISCUSSION

In light of mounting data documenting the success of various cancer immunotherapeutics and the recent clinical approval of the herpes simplex virus (HSV) expressing

A

Virus	Dose (TCID ₅₀)	Toxic events
rVSV	10 ³	0/3
	10 ⁴	0/3
	10 ⁵	3/3
	10 ⁶	3/3
rVSV-NDV	10 ⁴	0/3
	10 ⁵	0/3
	10 ⁶	0/3
	10 ⁷	1/6



B

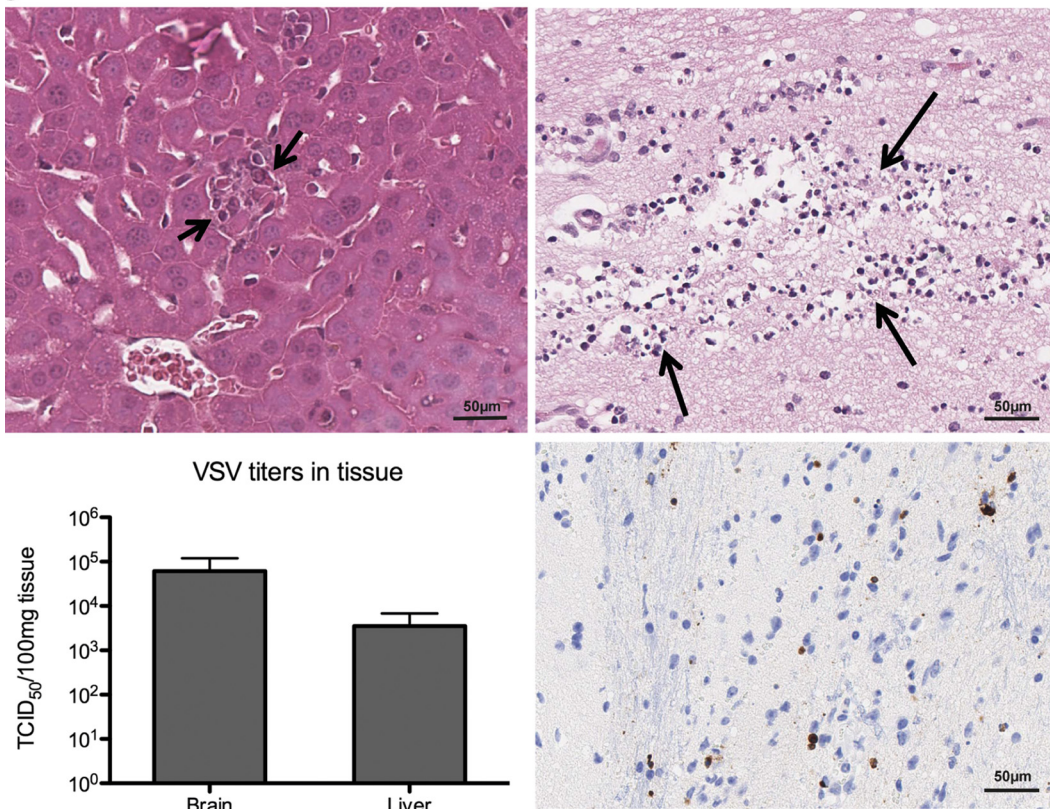


FIG 6 The maximum tolerated dose (MTD) of rVSV-NDV is elevated by 3 logs compared to that of rVSV in immunodeficient mice. Immunodeficient male NOD-SCID mice were treated by tail vein injection with increasing doses of rVSV-GFP or rVSV-NDV in a classic 3-plus-3 dosing scheme. Mice were monitored daily for the onset of dose-limiting toxicities and euthanized at humane endpoints. (A) A summary of the administered doses and of the occurrence of toxic events for each virus is shown in tabular form, as well as by a Kaplan-Meier survival curve. Red boxes in the graph legend indicate the respective MTD values for the viruses. (B) Hematoxylin-eosin staining of liver tissue revealed small-group necrosis of hepatocytes after rVSV treatment, marked by hepatocellular degeneration with karyolysis, as indicated by short black arrows (top left panel). Acute necrosis in the brain stem was observed after rVSV application, with degenerating glia cells exhibiting pyknosis and karyorrhexis, as indicated by long black arrows (top right panel) and by positive immunohistochemical staining (brown) for cleaved caspase-3 (bottom right). Representative images are shown; scale bars equal 50 μm. Viral titers were quantified in brain and liver tissue lysate obtained from mice receiving rVSV after demonstrating signs of toxicity (bottom left). Means + standard errors of the means (SEM) are shown.

granulocyte-macrophage colony-stimulating factor (GM-CSF), marketed as Imlytic, there is currently a surge of enthusiasm for the further development of improved viroimmunotherapeutics for cancer. Researchers now face the challenge of selecting an optimal vector platform to maximize direct oncolysis and immune-mediated effects while restricting off-target toxicity.

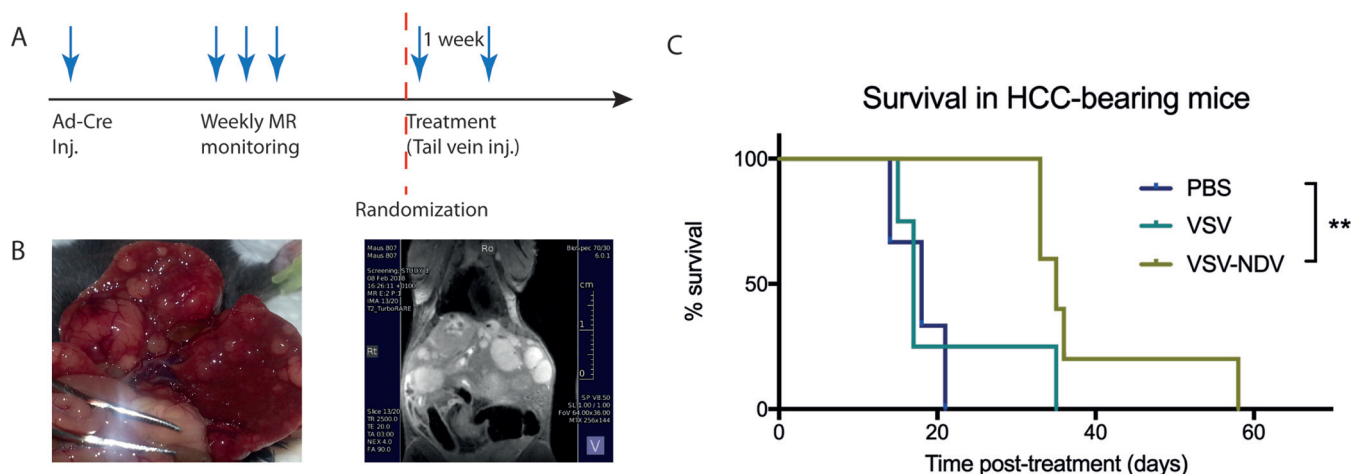


FIG 7 Tail vein injection of rVSV-NDV results in a significant survival prolongation in orthotopic, multifocal HCC-bearing mice. (A) Orthotopic HCC lesions were induced in male AST mice by injection of 2.5×10^8 PFU of rAd-Cre. Upon reaching the inclusion criteria, as determined by weekly magnetic resonance (MR) monitoring, mice were randomized to receive 2 weekly injections of rVSV-GFP, rVSV-NDV, or PBS. (B) The inducible HCC model results in heterogeneous, multifocal intrahepatic lesions that are visible macroscopically and also visible by T2-weighted magnetic resonance imaging (MRI) using a small-animal 7T MR device. (C) Mice were monitored daily and euthanized at humane endpoints. Survival times posttreatment were plotted as a Kaplan-Meier survival curve. Statistical significance was determined by the log rank test. P value for rVSV-NDV treatment versus PBS = 0.0042.

Vesicular stomatitis virus (VSV) represents an attractive oncolytic virus choice due to various advantageous features, such as a rapid replication cycle, the ability to infect a wide range of host cells and to produce high-titer stocks, the restriction of virus replication to the cell cytoplasm to avoid integration into host genomes, and a lack of preexisting immunity in most humans. Over the last decade, encouraging therapeutic effects have been reported, using numerous recombinant VSV vectors in a variety of tumor models (25). In particular, we have demonstrated promising survival prolongations with the application of rVSV by hepatic arterial delivery in orthotopic HCC-bearing rats (10, 12, 13, 26), and a phase I clinical trial of a VSV vector expressing human IFN- β is ongoing in patients with advanced refractory liver cancer (ClinicalTrials.gov identifier NCT1628640). However, despite these promising developments, the clinical translation of VSV as an oncolytic vector has been greatly hindered by its notoriously narrow therapeutic index, with the onset of dose-limiting neurotoxicity and hepatotoxicity when administered at elevated doses. To improve the safety of oncolytic VSV vectors, researchers have investigated a variety of approaches, including the modification of the matrix protein to enhance cellular antiviral responses (27, 28), the introduction of microRNA target sequences to alter the tropism of the virus (29, 30), and, more recently, the exchange of the targeting glycoprotein for that of a safer heterologous virus (31, 32). Although these approaches can be effective in reducing off-target replication of VSV, the cytopathic effects are also often attenuated in the target tumor cells.

In this study, we describe a novel chimeric vector in which the VSV glycoprotein has been replaced by the envelope proteins of oncolytic NDV. It has previously been reported that the introduction of a polybasic protease cleavage site into the fusion protein of the Hitchner B1 strain of NDV (rNDV/F3aa) allows efficient syncytium formation in a wide range of cells in the absence of exogenous proteases (33). We have demonstrated that further modification of the F3aa-modified fusion protein via a leucine-to-alanine substitution at amino acid 289 (L289A) caused substantially greater syncytial formation and tumor necrosis than was seen with the virus bearing only the F3aa mutation, without inducing any additional toxicity (11). We have also reported that the incorporation the gene encoding this modified hyperfusogenic F protein into the rVSV genome as an additional transcription unit resulted in cell-cell fusion and enhanced tumor cell killing. However, because the endogenous VSV G glycoprotein was also expressed in this construct, there was no effective mechanism in place for detargeting the brain or liver, and this vector was, therefore, no safer than the wild-type

VSV. In the current report, we describe, for the first time, a chimeric VSV-NDV vector in which the VSV-G was replaced by the hyperfusogenic F and HN proteins of NDV, which simultaneously addresses safety and efficacy issues.

By generating a hybrid of these two very promising oncolytic viruses, we hypothesized that the benefits would be 3-fold as follows. (i) The virus would be safe, both for the recipients and for the environment. (ii) The virus would spread efficiently from cell to cell. (iii) Immunogenic cell death would be induced by fusion-mediated syncytium formation. Off-target replication was shown to be minimized by the glycoprotein exchange, allowing substantially higher doses of virus to be administered without toxic effects (Fig. 6). Furthermore, this hybrid virus also appears to be safe in avian hosts. This can be explained by the fact that the pathogenicity of NDV in birds is a consequence of an avian species-specific IFN- α/β antagonist encoded by the viral V protein, which is a product of gene editing of the viral phosphoprotein (34, 35). As this gene was not included in our hybrid construct, rVSV-NDV was not expected to cause virulence in birds. Indeed, inoculation of embryonated chicken eggs with rVSV-NDV resulted in titers approximately 4-logs lower than that produced by rNDV (data not shown), and a mean death time assay indicated that the hybrid virus can be classified as lentogenic. By definition, this engineered vector is not expected to pose a threat to the environment, giving it a significant advantage over many oncolytic NDV vectors under development, which are primarily mesogenic strains.

By replacement of the VSV glycoprotein with the NDV envelope proteins, virus spread is mediated via direct cell-to-cell fusion, allowing efficient cytotoxic effects in tumor cells without the need for high virus titers. In fact, in the HCC cell lines, we observed a similar rate of tumor cell death *in vitro* upon infection with rVSV-NDV, despite substantially attenuated virus propagation compared to rVSV (Fig. 2). Moreover, due to the direct infection of neighboring cells through fusion, the virus remains primarily intracellular, an aspect that has several beneficial implications. First, because the virus remains predominantly intracellular, the risk of exposure to neutralizing antibodies and other antiviral immune mechanisms is minimized and could allow prolonged replication kinetics *in vivo* and, potentially, justify repeated intratumoral administrations of rVSV-NDV, even after the onset of neutralizing antibody responses. Furthermore, we speculate that by altering the mechanism of virus-mediated cytotoxicity to syncytium formation, we provide an additional mechanism of safety for the modified virus, since fewer infectious virus particles are produced and released into the surrounding tissue, which could potentially reduce or prevent viremia. This is in stark contrast to the results that we saw with our previously reported rVSV-F vector, in which the NDV fusion protein is expressed in addition to the endogenous VSV glycoprotein. Because both the VSV and the fusogenic NDV glycoproteins are expressed in the rVSV-F construct, the virus is able to replicate to very high titers and to spread both by classic CPE and by syncytium formation. Therefore, although use of this vector did result in enhanced efficacy in HCC through augmented viral spread, it did nothing to address safety, and, in fact, the MTD for rVSV-F was the same as for wild-type VSV (23).

Finally, our engineered vector causes infected cells to display markers of immunogenic cell death to a much greater extent than is achieved by cells infected with rVSV. By nature, viruses induce danger signals which result in the recruitment and activation of professional antigen-presenting cells, such as dendritic cells (DCs), which in turn can prime adaptive immune responses against specific tumor-associated antigens (TAAs). Syncytium formation that is induced by the expression of paramyxoviral fusogenic glycoproteins is known to trigger efficient presentation of TAAs by DCs (36), thus leading to immunogenic cell death. Viruses expressing fusion proteins therefore act as immune adjuvants to overcome the typically immunosuppressive tumor microenvironment, as these infected cells expose or release danger-associated molecular patterns (DAMPs) (37), such as the expression of ecto-CRT and the release of ATP, HMGB1, Hsp70, and Hsp90, as demonstrated here (Fig. 5). This implies that *in vivo* therapy with fusogenic rVSV-NDV could provide an additional therapeutic mechanism through enhanced induction of adaptive immune responses directed against the tumor. Fur-

thermore, it is possible to introduce additional foreign genes into the rVSV-NDV backbone without causing additional attenuation of the virus (data not shown), indicating that the incorporation of immune-stimulating genes and the use of this vector as a vaccine platform would be feasible options to further improve the therapeutic utility of the oncolytic virus.

Our preliminary *in vivo* efficacy studies demonstrated that the rVSV-NDV platform is effective at prolonging survival of immunocompetent mice bearing orthotopic, multifocal HCC. This was especially striking given the fact that the virus was administered systemically, a route which is known to be inefficient for delivering oncolytic viruses to their tumor targets. Although additional mechanistic studies are necessary to investigate the mechanism for the observed response, we hypothesize that the fusogenic capacity of the virus circumvents the need for high titers of virus to accumulate within the tumor, since single virions have the capacity to kill multiple cells through syncytium formation and subsequent immunogenic cell death. We further speculate that administration of higher doses of rVSV-NDV, which are enabled by the enhanced safety, will result in even more impressive therapeutic responses and survival outcomes. This aspect will be addressed in future investigations.

Recently, those oncolytic viruses that encode a fusion protein, either endogenously or via viral engineering, have entered the spotlight as optimal therapeutic candidates for their abilities to combine the benefits of direct oncolytic activity and superior immune stimulation (9). In particular, the envelope proteins of paramyxoviruses show great promise as components of OV platforms. Paramyxovirus infection is coordinated by the activities of two envelope glycoproteins: an attachment (hemagglutinin-neuraminidase [HN]) protein and a fusion protein. An additional attractive feature of these viruses is that the HN protein attaches to target cells via molecules containing sialic acid residues, providing a convenient intrinsic targeting mechanism, as tumor cells tend to overexpress sialoglycoproteins on their surface (38, 39). Furthermore, it is thought that the sialidase activity of HN could offer a unique immune-stimulating benefit through the removal of sialic acid residues from the surface of cancer cells. The relatively high density of sialic acid glycoproteins has been correlated with the invasive potential of a tumor by shielding tumor antigens and providing an immune escape mechanism (37, 40, 41). Sialidase activity has been shown to stimulate natural killer (NK) cell activity and induce T cell responses (42, 43). Therefore, the HN expression mediated by the rVSV-NDV construct could provide the additional therapeutic benefit of NK cell and T cell activation.

In anticipation of the further development of rVSV-NDV for clinical application, the manufacturability of the vector is an important consideration. Our growth kinetics data in Huh7 and HepG2 cells highlight the challenge encountered in efforts to produce high titers of this virus, due to the rapid and efficient fusogenicity of infected cells, which results in cell death before high titers can be reached. Nevertheless, we managed to develop an optimized production protocol in the AGE1.CR Muscovy duck cell line, which allowed us to produce titers of up to 3×10^8 TCID₅₀/ml. For our purposes, this titer was sufficient for carrying out experiments in mice, but we anticipate that further optimization steps and scaling up of the production process will allow us to manufacture the high-titer stocks necessary for clinical studies.

In conclusion, this report represents a critical step toward the establishment of an optimal vector platform that is safe and potentially extremely effective. The data presented here indicate that chimeric VSV-NDV will be at least as efficient in killing HCC as rVSV is, and, with a significantly enhanced safety profile, it allows higher doses to be applied without inducing dose-limiting side effects. *In vivo* efficacy will be further characterized in preclinical investigations that are under way. Moreover, although our current therapeutic target is HCC, there is nothing inherently HCC specific about this vector, and it has the potential to be effective in many other tumor settings, which will also be investigated in follow-up studies. We therefore suggest, for the many reasons discussed here, that rVSV-NDV represents an extremely promising platform for future development as a viroimmunotherapeutic for clinical translation as an effective and safe cancer therapy.

MATERIALS AND METHODS

Viruses. Recombinant VSV vectors expressing the green fluorescent protein (GFP) reporter (referred to here as “rVSV”) or the modified NDV-F(L289A) protein (referred to here as “rVSV-F”) were previously described (23, 44). Stocks were produced in baby hamster kidney cells (BHK-21) and purified by sucrose gradient, in accordance with our previously established protocol (10). Recombinant NDV harboring the F3aa(L289A) mutation and expressing the GFP reporter gene [rNDV/F3aa(L289A)-GFP] (referred to here as “rNDV”) was engineered and rescued as previously described (11). The virus was amplified in embryonated pathogen-free chicken eggs (Charles River Laboratories) and purified by the use of a sucrose gradient as previously described (11).

Recombinant rVSV-NDV was produced by first modifying a plasmid carrying the full-length VSV genome (pVSV-XN2) and expressing the F3aa(L289A)-modified fusion protein of NDV as an additional transcription unit between VSV's glycoprotein (G) and large polymerase (L) genes (23). The endogenous G was then deleted by digestion with MluI and XhoI restriction enzymes, which recognize the unique restriction sites in the 5' and 3' noncoding regions of G, respectively. Following blunting and self-ligation of the G-deleted plasmid, a short oligonucleotide linker was inserted at the unique NheI restriction site following the NDV F gene to create a multiple cloning site for insertion of the HN gene. The HN gene was amplified by PCR from a plasmid carrying the full-length NDV genome, utilizing primers to introduce PacI and PmeI restriction sites at the 5' and 3' ends of the PCR product, respectively, for insertion into the newly incorporated restriction sites in the G-deleted VSV-NDV/F3aa(L289A) plasmid (see Fig. 1 for the final construct). The resulting plasmid was subjected to sequence analysis to confirm the fidelity of the PCR insertion, as well as the intergenic transcription start and stop sequences and the gene order. Finally, the infectious virus, referred to here as “rVSV-NDV,” was rescued using the established reverse genetics system for rescuing negative-strand RNA viruses (45) with a slight modification in that a plasmid encoding the VSV-G protein was cotransfected along with the standard rescue plasmids encoding the nucleocapsid (N), phosphoprotein (P), and L. Virus stocks for *in vitro* experiments were concentrated from BHK-21 cell lysates and supernatants using Amicon Ultra centrifugal filters (Merck-Millipore, Burlington, MA) with a 100-kDa size cutoff and purified by sucrose gradient as previously described (10). Stocks for *in vivo* experiments were produced in AGE1.CR cells (ProBioGen AG, Berlin, Germany) and concentrated by ultracentrifugation, followed by purification on sucrose gradients.

Cell lines and primary cell culture. BHK-21 cells were purchased from the American Type Culture Collection (ATCC, Rockville, MD) and were maintained in Glasgow minimum essential medium (GMEM) (Gibco, Carlsbad, CA) supplemented with 10% fetal bovine serum (FBS). Two human HCC cell lines (HepG2 and Huh7) were obtained from Ulrich Lauer (University Hospital Tübingen, Tübingen, Germany) and maintained in Dulbecco's modified Eagle's medium (DMEM) supplemented with 10% FBS, 2 mM L-glutamine, and 1 mM sodium pyruvate, as well as penicillin/streptomycin and nonessential amino acids. A549 cells were obtained from the ATCC and cultured in the same medium as the HCC cell lines. AGE1.CR cells (ProBioGen AG, Berlin, Germany) were cultured in DMEM/F12 medium containing L-glutamine (Biowest, Nuaille, France) supplemented with 5% FBS and penicillin/streptomycin. Primary human hepatocytes (PHH) were derived from patients (negative for hepatitis B and C virus and human immunodeficiency virus) who had undergone surgical resection of liver tumors, in accordance with the guidelines of the charitable state-controlled Human Tissue and Cell Research (HTCR) foundation (Regensburg, Germany) (46). The hepatocytes were isolated using a two-step collagenase perfusion technique, as previously described (47), and were maintained in HepatoZYME-SFM medium (Gibco-Invitrogen, Karlsruhe, Germany). Primary embryonic cortical neurons were dissociated from E16.5 C57/Bl6 mouse embryos as previously described (48). This procedure was performed in accordance with the European Communities Council Directive (2010/63/EU) and in compliance with the German animal welfare law. Neuronal cultures were maintained in neurobasal medium (Gibco) supplemented with 2% B-27 (Thermo Fisher Scientific, Waltham, MA), 0.5 mM L-glutamine, and 1% penicillin/streptomycin. All cell lines and primary cells were maintained in a 37°C humidified incubator with 5% CO₂.

Indirect immunofluorescence assay. Huh7 cells were plated at a density of 10⁵ cells per well in 8-well chamber slides (Corning Life Sciences, Corning, NY). Wells were mock infected or infected with rVSV, rNDV, or rVSV-NDV in duplicate at a multiplicity of infection (MOI) of 0.001 for 24 h. For detection of viral proteins, the cells were fixed for 15 min in 4% paraformaldehyde (PFA) prior to indirect immunofluorescent analysis using antibodies against VSV-G (Rockland Immunochemicals, Limerick, PA), VSV-M (matrix protein) (Kerafast Inc., Boston, MA), and NDV-HN (Santa Cruz Biotechnology, Santa Cruz, CA) with appropriate fluorochrome-labeled secondary antibodies (Jackson ImmunoResearch, West Grove, PA). Cells were counterstained with DAPI (4',6-diamidino-2-phenylindole) for localization of nuclei. For detection of ecto-CRT, live cells in culture were incubated with a monoclonal rabbit anti-CRT antibody (Cell Signaling Technology, Danvers, MA) for 1 h at 37°C, washed 3 times with phosphate-buffered saline (PBS), and then incubated with a fluorescein isothiocyanate (FITC)-conjugated goat anti-rabbit secondary antibody (Jackson ImmunoResearch, West Grove, PA) diluted in fresh cell medium. After washing, cell membranes were labeled using CellMask Deep Red (Thermo Fisher Scientific, Waltham, MA) according to the manufacturer's instructions. Finally, cells were fixed for 15 min with 4% PFA and mounted with Fluoroshield mounting medium (Abcam, Cambridge, United Kingdom). Representative images were captured under ×400 magnification on an Axio Imager (Carl Zeiss, Jena, Germany).

Growth curves. Viral growth curves were analyzed in HCC cell lines (Huh7 and HepG2), as well as in primary human hepatocytes and primary mouse neurons. HCC cell lines were plated in 6-well dishes at a density of 3.5 × 10⁵ cells per well, while PHH and neurons were seeded in collagen-coated 24-well dishes at a density of 10⁵ cells per well. Each cell line was infected with rVSV, rNDV, or rVSV-NDV at an MOI of 0.01. The infections were performed in 1 ml (6-well dishes) or 250 μl (24-well dishes) of PBS at 37°C for 1 h. After incubation, cells were washed three times with PBS, and fresh medium was added. Cell monolayers were

collected by scraping in PBS at 0, 16, 24, 48, and 72 h postinfection and lysed by 3 cycles of freezing and thawing. Intracellular virus titers were measured with a 50% tissue culture infective dose (TCID₅₀) assay.

Cytotoxicity assays. Cell viability of infected HCC cell lines (Huh7 and HepG2) and primary human hepatocytes was analyzed by measuring levels of released lactate dehydrogenase (LDH) in cell culture supernatant. The cells were plated, infected, and washed as described for the growth curve experiments. At 24, 48, and 72 h postinfection, aliquots of supernatant were collected, and LDH release was quantified using the CytoTox 96 nonradioactive cytotoxicity assay protocol (Promega, Madison, WI). For each time point, LDH release following virus infection was calculated as a percentage of the maximum control LDH release. Baseline LDH levels detected in the supernatant of mock-treated cells were subtracted from the values obtained from the experimental wells.

Cell viability of neurons was analyzed with an MTS [3-(4,5-dimethylthiazol-2-yl)-5-(3-carboxymethoxyphenyl)-2-(4-sulfophenyl)-2H-tetrazolium] assay using the CellTiter 96 AQueous One Solution cell proliferation assay (Promega). Neurons were seeded in collagen-coated 96-well dishes at a density of 5×10^4 cells per well and mock treated or infected with rVSV, rNDV, or rVSV-NDV at an MOI of 0.01. At 24, 48, and 72 h postinfection, cell viability was measured according to the manufacturer's protocol. Cytotoxicity was quantified as the difference in cell viability between the experimental samples and the uninfected controls.

Microscopic analysis of cultured cells. Huh7 and HepG2 cells were plated at approximately 90% confluence in 6-well dishes and mock infected or infected with rVSV or rNDV or rVSV-NDV at an MOI of 0.01. Cells were visualized at $\times 200$ magnification on an Axiovert 40CFL microscope (Zeiss) at 18, 24, and 48 h postinfection, and representative images were captured with an AxioCam ICm1 camera (Carl Zeiss) attached to the microscope.

Interferon protection assay. Interferon-sensitive A549 cells were plated in 24-well dishes at a density of 10^5 cells per well and cultured overnight. The following evening, they were pretreated with different concentrations (0, 100, 500, and 1,000 IU/ml) of universal type I interferon (IFN) added directly to the culture medium. After overnight incubation, fresh medium containing IFN was added, and the cells were infected with rVSV or rNDV or rVSV-NDV at an MOI of 0.01. Cells were collected in 100 μ l of PBS at 48 h postinfection and lysed by three freeze-thaw cycles. The intratumoral virus titer was determined by TCID₅₀ analysis of the cell lysates.

Mean death time assay. Specific-pathogen-free (SPF) embryonated chicken eggs (Charles River, Sulzfeld, Germany) (10 days old) were inoculated with 100 μ l of rNDV-GFP or rVSV-NDV in serial 10-fold dilutions, ranging from 10 to 10,000 TCID₅₀, with 5 eggs per virus dose. The eggs were incubated in a humidified 37°C incubator and monitored twice daily by candling for 7 days, and the time at which each embryo was found dead was recorded. The highest dilution that resulted in death of all embryos was considered to represent the minimum lethal dose (MLD). The mean death time (MDT) was calculated as the mean amount of time required for the embryos to be killed at the MLD.

Western blotting. Huh7 cells were plated in 6-well plates at approximately 90% confluence and mock infected or infected with rVSV or rNDV or rVSV-NDV at an MOI of 0.01 for 48 h. The conditioned media were collected and concentrated to about 200 μ l using Amicon Ultra centrifugal filters (Merck Millipore, Billerica, MA) with a 10-kDa cutoff. Protein concentrations were quantified using the Pierce bicinchoninic acid (BCA) protein assay (Thermo Fisher Scientific, Waltham, MA), and 10 μ g of each sample was loaded onto a 7.5% denaturing sodium dodecyl sulfate-polyacrylamide gel electrophoresis (SDS-PAGE) gel before being transferred onto a nitrocellulose membrane. Protein bands were detected using specific antibodies against HMGB1 and Hsp90 (Cell Signaling Technology, Danvers, MA) as well as against Hsp70 (Santa Cruz Biotechnology, Dallas, TX) and the appropriate secondary antibody conjugated with horseradish peroxidase (Jackson ImmunoResearch, West Grove, PA). Bands were visualized using an Amersham ECL Prime Western blot detection kit (GE Healthcare Life Sciences, Marlborough, MA).

ATP release assay. Huh7 cells were plated at a density of 2×10^5 cells per well in 48-well plates prior to mock infection or infection with rVSV or rNDV or rVSV-NDV at an MOI of 0.01. Released ATP was measured in conditioned supernatants after a 24-h infection using an ATP CLS II bioluminescence assay kit (Roche, Indianapolis, IN) according to the manufacturer's instructions. Bioluminescence was measured using a single-tube luminometer (Turner Designs, Sunnyvale, CA), and ATP concentrations were calculated from a log-log plot of standard curve data.

Animal studies. All animal interventions were performed in accordance with protocols that were approved by the Center for Preclinical Research, Klinikum rechts der Isar, and the regional government commission for animal protection (Regierung von Oberbayern, Munich, Germany). Immune-deficient male NOD.CB17-prkdc^{scid}/NCRcr1 (NOD-SCID) mice of approximately 8 weeks of age were treated by tail vein injection with either rVSV-NDV or the control rVSV at increasing doses, using a 3-plus-3 Fibonacci dose escalation scheme (49). Mice were monitored daily for body weight and overall physical appearance, and they were euthanized at humane endpoints. Blood was sampled on days 1, 3, 7, and 14 and at the time of euthanization for analysis of viral titers and for serum chemistry measurements. Samples of brain and liver tissue were collected from euthanized mice and flash-frozen or prepared for histological analysis. Surviving mice were euthanized at 4 weeks postinjection for sampling of tissue and blood. Frozen samples were homogenized in PBS using glass Dounce tissue grinders and subjected to TCID₅₀ analysis. Titers were normalized to tissue weight.

For efficacy studies, transgenic AST mice, which harbor a construct consisting of the liver-specific albumin promoter, a loxP-flanked stop cassette, and the SV40 large T antigen, as an oncogene (50), were employed. To induce orthotopic HCC, an adenovirus vector expressing cre recombinase (SigmaGen Laboratories, Rockville, MD) was injected via tail vein at a dose of 2.5×10^8 PFU in male mice of 6 to 8 weeks of age. At approximately 5 weeks postinjection, the mice were subjected to weekly anatomical

scans by magnetic resonance imaging (MRI) for screening of HCC development. When the predetermined inclusion criteria were reached (a single nodule of at least 5 mm in diameter or multiple nodules with a minimum diameter of 2 mm, resulting in an additive tumor diameter of at least 5 mm), mice were randomized for treatment by tail vein injection with rVSV-GFP ($n = 4$) or rVSV-NDV ($n = 5$) at a dose of 10^7 TCID₅₀, or with PBS ($n = 3$), in a 200- μ l volume. Treatments were administered twice, with a 1-week interval between injections. Mice were monitored daily and euthanized at humane endpoints due to tumor burden. Survival times with respect to the first injection of treatment were plotted as a Kaplan-Meier survival curve, and mean survival times were calculated.

Magnetic resonance imaging. Abdominal anatomical T2-weighted images were acquired with a 7T magnetic resonance imaging (MRI) system (Agilent/GE MR901 magnet with Bruker Avance III HD electronics), using a two-channel flexible array surface receive coil (RAPID Biomedical) placed over the mice, and a 72-mm-inner-diameter birdcage resonator for radiofrequency (RF) transmission. A fast spin echo (FSE) sequence was used with the following parameters: repetition time (TR) of 2,500 ms, echo time (TE) of 20 ms, 4 averages, 8 echoes per excitation, 20 horizontal slices of 1-mm thickness, matrix size of 256×144 , field of view (FOV) of 64×36 mm², fat suppression enabled, receive bandwidth of 100 kHz (without breath gating), and total acquisition time of 3 min. Animals were anesthetized with isoflurane during imaging.

Histology and immunohistochemistry. Tissue sections were fixed overnight in 4% paraformaldehyde and subsequently dehydrated and embedded in paraffin. Slices (3 μ m in thickness) were stained with hematoxylin-eosin or subjected to immunohistochemical staining using a rabbit monoclonal antibody against cleaved caspase-3 (Cell Signaling Technology, Danvers, MA) on a Bond RX automated staining instrument (Leica, Wetzlar, Germany). Analysis of pathological changes and confirmation of positive immunohistochemical reaction were performed by a certified pathologist who was blind to the treatment groups of the specimens.

Statistical analysis. Data were plotted and analyzed using GraphPad Prism 7.0 (GraphPad Software, San Diego, CA). Individual data points were compared for statistical significance using a two-sided Student's *t* test, and *P* values of less than 0.05 were considered to be statistically significant. Means and standard errors of the means (SEM) were plotted. Statistical significance of survival proportions was calculated by log rank test.

ACKNOWLEDGMENTS

We thank Adolfo García-Sastre (Mount Sinai School of Medicine, NY) for providing the NDV/F3aa construct and the NDV rescue system and Maresa Demmel and other members of the HCR for their seamless support in providing primary human hepatocytes. We also thank ProBioGen AG (Berlin, Germany) for providing AGE.CR1 cells and cultivation protocols, as well as for helpful discussions regarding virus production.

Funding for this work was provided by Sonderforschungsbereich (SFB) 824, sub-projects C7 (J.A.) and Z2 (K.S.), and by project FOR2290 (S.F.L.) from the German Research Foundation, Bonn, Germany, and the Centers of Excellence in Neurodegeneration program.

REFERENCES

1. Ferlay J, Soerjomataram I, Dikshit R, Eser S, Mathers C, Rebelo M, Parkin DM, Forman D, Bray F. 2015. Cancer incidence and mortality worldwide: sources, methods and major patterns in GLOBOCAN 2012. *Int J Cancer* 136:E359–E386. <https://doi.org/10.1002/ijc.29210>.
2. Coffey MC, Strong JE, Forsyth PA, Lee PW. 1998. Reovirus therapy of tumors with activated Ras pathway. *Science* 282:1332–1334. <https://doi.org/10.1126/science.282.5392.1332>.
3. Kirn D, Martuza RL, Zwiebel J. 2001. Replication-selective virotherapy for cancer: biological principles, risk management, and future directions. *Nat Med* 7:781–787. <https://doi.org/10.1038/89901>.
4. Peng KW, Ahmann GJ, Pham L, Greipp PR, Cattaneo R, Russell SJ. 2001. Systemic therapy of myeloma xenografts by an attenuated measles virus. *Blood* 98:2002–2007. <https://doi.org/10.1182/blood.V98.7.2002>.
5. Lorence RM, Katubig BB, Reichard KW, Reyes HM, Phuangsab A, Sasseti MD, Walter RJ, Peeples ME. 1994. Complete regression of human fibrosarcoma xenografts after local Newcastle disease virus therapy. *Cancer Res* 54:6017–6021.
6. Melzer MK, Lopez-Martinez A, Altomonte J. 2017. Oncolytic vesicular stomatitis virus as a viro-immunotherapy: defeating cancer with a “hammer” and “anvil”. *Biomedicines* 5:8. <https://doi.org/10.3390/biomedicines5010008>.
7. Melcher A, Parato K, Rooney CM, Bell JC. 2011. Thunder and lightning: immunotherapy and oncolytic viruses collide. *Mol Ther* 19:1008–1016. <https://doi.org/10.1038/mt.2011.65>.
8. Ledford H. 2015. Cancer-fighting viruses win approval. *Nature* 526:622–623. <https://doi.org/10.1038/526622a>.
9. Krabbe T, Altomonte J. 2018. Fusogenic viruses in oncolytic immunotherapy. *Cancers (Basel)* 10:216. <https://doi.org/10.3390/cancers10070216>.
10. Altomonte J, Braren R, Schulz S, Marozin S, Rummeny EJ, Schmid RM, Ebert O. 2008. Synergistic antitumor effects of transarterial viroembolization for multifocal hepatocellular carcinoma in rats. *Hepatology* 48:1864–1873. <https://doi.org/10.1002/hep.22546>.
11. Altomonte J, Marozin S, Schmid RM, Ebert O. 2010. Engineered Newcastle disease virus as an improved oncolytic agent against hepatocellular carcinoma. *Mol Ther* 18:275–284. <https://doi.org/10.1038/mt.2009.231>.
12. Altomonte J, Wu L, Chen L, Meseck M, Ebert O, Garcia-Sastre A, Fallon J, Woo SL. 2008. Exponential enhancement of oncolytic vesicular stomatitis virus potency by vector-mediated suppression of inflammatory responses in vivo. *Mol Ther* 16:146–153. <https://doi.org/10.1038/sj.mt.6300343>.
13. Altomonte J, Wu L, Meseck M, Chen L, Ebert O, Garcia-Sastre A, Fallon J, Mandeli J, Woo SL. 2009. Enhanced oncolytic potency of vesicular stomatitis virus through vector-mediated inhibition of NK and NKT cells. *Cancer Gene Ther* 16:266–278. <https://doi.org/10.1038/cgt.2008.74>.
14. van den Pol A, Dalton K, Rose J. 2002. Relative neurotropism of a recombinant rhabdovirus expressing a green fluorescent envelope glycoprotein. *J Virol* 76:1309–1327. <https://doi.org/10.1128/JVI.76.3.1309-1327.2002>.
15. Johnson JE, Nasar F, Coleman JW, Price RE, Javadian A, Draper K, Lee M, Reilly PA, Clarke DK, Hendry RM, Udem SA. 2007. Neurovirulence properties of recombinant vesicular stomatitis virus vectors in non-human primates. *Virology* 360:36–49. <https://doi.org/10.1016/j.virol.2006.10.026>.

16. Zhang L, Steele MB, Jenks N, Grell J, Sukanpaisan L, Naik S, Federspiel MJ, Lacy MQ, Russell SJ, Peng KW. 2016. Safety studies in tumor and non-tumor-bearing mice in support of clinical trials using oncolytic VSV-IFNbeta-NIS. *Hum Gene Ther Clin Dev* 27:111–122. <https://doi.org/10.1089/humc.2016.061>.
17. Quiroz E, Moreno N, Peralta PH, Tesh RB. 1988. A human case of encephalitis associated with vesicular stomatitis virus (Indiana serotype) infection. *Am J Trop Med Hyg* 39:312–314. <https://doi.org/10.4269/ajtmh.1988.39.312>.
18. Freeman AI, Zakay-Rones Z, Gomori JM, Linetsky E, Rasooly L, Greenbaum E, Rozenman-Yair S, Panet A, Libson E, Irving CS, Galun E, Siegal T. 2006. Phase I/II trial of intravenous NDV-HUJ oncolytic virus in recurrent glioblastoma multiforme. *Mol Ther* 13:221–228. <https://doi.org/10.1016/j.jymthe.2005.08.016>.
19. Schirmmacher V. 2005. Clinical trials of antitumor vaccination with an autologous tumor cell vaccine modified by virus infection: improvement of patient survival based on improved antitumor immune memory. *Cancer Immunol Immunother* 54:587–598. <https://doi.org/10.1007/s00262-004-0602-0>.
20. Cuadrado-Castano S, Sanchez-Aparicio MT, Garcia-Sastre A, Villar E. 2015. The therapeutic effect of death: Newcastle disease virus and its antitumor potential. *Virus Res* 209:56–66. <https://doi.org/10.1016/j.virusres.2015.07.001>.
21. Kroemer G, Galluzzi L, Kepp O, Zitvogel L. 2013. Immunogenic cell death in cancer therapy. *Annu Rev Immunol* 31:51–72. <https://doi.org/10.1146/annurev-immunol-032712-100008>.
22. Workenhe ST, Mossman KL. 2014. Oncolytic virotherapy and immunogenic cancer cell death: sharpening the sword for improved cancer treatment strategies. *Mol Ther* 22:251–256. <https://doi.org/10.1038/mt.2013.220>.
23. Ebert O, Shinozaki K, Kournioti C, Park MS, Garcia-Sastre A, Woo SL. 2004. Syncytia induction enhances the oncolytic potential of vesicular stomatitis virus in virotherapy for cancer. *Cancer Res* 64:3265–3270. <https://doi.org/10.1158/0008-5472.CAN-03-3753>.
24. Shin EJ, Chang JI, Choi B, Wanna G, Ebert O, Genden EM, Woo SL. 2007. Fusogenic vesicular stomatitis virus for the treatment of head and neck squamous carcinomas. *Otolaryngol Head Neck Surg* 136:811–817. <https://doi.org/10.1016/j.otohns.2006.11.046>.
25. Hastie E, Grdzlishvili VZ. 2012. Vesicular stomatitis virus as a flexible platform for oncolytic virotherapy against cancer. *J Gen Virol* 93:2529–2545. <https://doi.org/10.1099/vir.0.046672-0>.
26. Altomonte J, Munoz-Alvarez KA, Shinozaki K, Baumgartner C, Kaissis G, Braren R, Ebert O. 2016. Transarterial administration of oncolytic viruses for locoregional therapy of orthotopic HCC in rats. *J Vis Exp* <https://doi.org/10.3791/53757>.
27. Ebert O, Harbaran S, Shinozaki K, Woo SL. 2005. Systemic therapy of experimental breast cancer metastases by mutant vesicular stomatitis virus in immune-competent mice. *Cancer Gene Ther* 12:350–358. <https://doi.org/10.1038/sj.cgt.7700794>.
28. Stojdl DF, Lichty BD, tenOever BR, Paterson JM, Power AT, Knowles S, Marius R, Reynard J, Poliquin L, Atkins H, Brown EG, Durbin RK, Durbin JE, Hiscott J, Bell JC. 2003. VSV strains with defects in their ability to shutdown innate immunity are potent systemic anti-cancer agents. *Cancer Cell* 4:263–275. [https://doi.org/10.1016/S1535-6108\(03\)00241-1](https://doi.org/10.1016/S1535-6108(03)00241-1).
29. Edge RE, Falls TJ, Brown CW, Lichty BD, Atkins H, Bell JC. 2008. A let-7 MicroRNA-sensitive vesicular stomatitis virus demonstrates tumor-specific replication. *Mol Ther* 16:1437–1443. <https://doi.org/10.1038/mt.2008.130>.
30. Kelly EJ, Nace R, Barber GN, Russell SJ. 2010. Attenuation of vesicular stomatitis virus encephalitis through microRNA targeting. *J Virol* 84:1550–1562. <https://doi.org/10.1128/JVI.01788-09>.
31. Muik A, Kneiske I, Werbizki M, Wilflingseder D, Giroglou T, Ebert O, Kraft A, Dietrich U, Zimmer G, Momma S, von Laer D. 2011. Pseudotyping vesicular stomatitis virus with lymphocytic choriomeningitis virus glycoproteins enhances infectivity for glioma cells and minimizes neurotropism. *J Virol* 85:5679–5684. <https://doi.org/10.1128/JVI.02511-10>.
32. Ayala-Breton C, Barber GN, Russell SJ, Peng KW. 2012. Retargeting vesicular stomatitis virus using measles virus envelope glycoproteins. *Hum Gene Ther* 23:484–491. <https://doi.org/10.1089/hum.2011.146>.
33. Vigil A, Park M-S, Martinez O, Chua MA, Xiao S, Cros JF, Martinez-Sobrido L, Woo SLC, Garcia-Sastre A. 2007. Use of reverse genetics to enhance the oncolytic properties of Newcastle disease virus. *Cancer Res* 67:8285–8292. <https://doi.org/10.1158/0008-5472.CAN-07-1025>.
34. Huang Z, Krishnamurthy S, Panda A, Samal SK. 2003. Newcastle disease virus V protein is associated with viral pathogenesis and functions as an alpha interferon antagonist. *J Virol* 77:8676–8685. <https://doi.org/10.1128/JVI.77.16.8676-8685.2003>.
35. Park MS, Garcia-Sastre A, Cros JF, Basler CF, Palese P. 2003. Newcastle disease virus V protein is a determinant of host range restriction. *J Virol* 77:9522–9532. <https://doi.org/10.1128/JVI.77.17.9522-9532.2003>.
36. Bateman AR, Harrington KJ, Kottke T, Ahmed A, Melcher AA, Gough MJ, Linardakis E, Riddle D, Dietz A, Lohse CM, Strome S, Peterson T, Simari R, Vile RG. 2002. Viral fusogenic membrane glycoproteins kill solid tumor cells by nonapoptotic mechanisms that promote cross presentation of tumor antigens by dendritic cells. *Cancer Res* 62:6566–6578.
37. Matveeva OV, Guo ZS, Shabalina SA, Chumakov PM. 2015. Oncolysis by paramyxoviruses: multiple mechanisms contribute to therapeutic efficiency. *Mol Ther Oncolytics* 2:15011. <https://doi.org/10.1038/mto.2015.11>.
38. Bull C, Stoel MA, den Brok MH, Adema GJ. 2014. Sialic acids sweeten a tumor's life. *Cancer Res* 74:3199–3204. <https://doi.org/10.1158/0008-5472.CAN-14-0728>.
39. Bull C, den Brok MH, Adema GJ. 2014. Sweet escape: sialic acids in tumor immune evasion. *Biochim Biophys Acta* 1846:238–246. <https://doi.org/10.1016/j.bbcan.2014.07.005>.
40. Pearlstein E, Salk PL, Yogeewaran G, Karpatkin S. 1980. Correlation between spontaneous metastatic potential, platelet-aggregating activity of cell surface extracts, and cell surface sialylation in 10 metastatic-variant derivatives of a rat renal sarcoma cell line. *Proc Natl Acad Sci U S A* 77:4336–4339. <https://doi.org/10.1073/pnas.77.7.4336>.
41. Yogeewaran G, Salk PL. 1981. Metastatic potential is positively correlated with cell surface sialylation of cultured murine tumor cell lines. *Science* 212:1514–1516. <https://doi.org/10.1126/science.7233237>.
42. Cohen M, Elkabets M, Perlmutter M, Porgador A, Voronov E, Apte RN, Lichtenstein RG. 2010. Sialylation of 3-methylcholanthrene-induced fibrosarcoma determines antitumor immune responses during immunoeediting. *J Immunol* 185:5869–5878. <https://doi.org/10.4049/jimmunol.1001635>.
43. Powell LD, Whiteheart SW, Hart GW. 1987. Cell surface sialic acid influences tumor cell recognition in the mixed lymphocyte reaction. *J Immunol* 139:262–270.
44. Huang TG, Ebert O, Shinozaki K, Garcia-Sastre A, Woo SL. 2003. Oncolysis of hepatic metastasis of colorectal cancer by recombinant vesicular stomatitis virus in immune-competent mice. *Mol Ther* 8:434–440. [https://doi.org/10.1016/S1525-0016\(03\)00204-1](https://doi.org/10.1016/S1525-0016(03)00204-1).
45. Lawson ND, Stillman EA, Whitt MA, Rose JK. 1995. Recombinant vesicular stomatitis viruses from DNA. *Proc Natl Acad Sci U S A* 92:4477–4481. <https://doi.org/10.1073/pnas.92.10.4477>.
46. Thasler WE, Weiss TS, Schillhorn K, Stoll PT, Irrgang B, Jauch KW. 2003. Charitable state-controlled foundation human tissue and cell research: ethic and legal aspects in the supply of surgically removed human tissue for research in the academic and commercial sector in Germany. *Cell Tissue Bank* 4:49–56. <https://doi.org/10.1023/A:1026392429112>.
47. Lee SM, Schelcher C, Demmel M, Hauner M, Thasler WE. 2013. Isolation of human hepatocytes by a two-step collagenase perfusion procedure. *J Vis Exp* <https://doi.org/10.3791/50615>.
48. Kuhn PH, Wang H, Dislich B, Colombo A, Zeitschel U, Ellwart JW, Kremmer E, Rossner S, Lichtenthaler SF. 2010. ADAM10 is the physiologically relevant, constitutive alpha-secretase of the amyloid precursor protein in primary neurons. *EMBO J* 29:3020–3032. <https://doi.org/10.1038/emboj.2010.167>.
49. Le Tourneau C, Lee JJ, Siu LL. 2009. Dose escalation methods in phase I cancer clinical trials. *J Natl Cancer Inst* 101:708–720. <https://doi.org/10.1093/jnci/djp079>.
50. Stahl S, Sacher T, Bechtold A, Protzer U, Ganss R, Hammerling GJ, Arnold B, Garbi N. 2009. Tumor agonist peptides break tolerance and elicit effective CTL responses in an inducible mouse model of hepatocellular carcinoma. *Immunol Lett* 123:31–37. <https://doi.org/10.1016/j.imlet.2009.01.011>.